Interaction of three-finger toxins with phospholipid membranes: comparison of S- and P-type cytotoxins

Peter V. DUBOVSKII, Dmitry M. LESOVOY, Maxim A. DUBINNYI, Anastasiya G. KONSHINA, Yuri N. UTKIN, Roman G. EFREMOV and Alexander S. ARSENIEV[1]

Shemyakin and Ovchinnikov Institute of Bioorganic Chemistry, Russian Academy of Sciences, 16/10 Miklukho-Maklaya str., V-437, Moscow 117997, Russia

The CTs (cytotoxins) I and II are positively charged three-finger folded proteins from venom of *Naja oxiana* (the Central Asian cobra). They belong to S- and P-type respectively based on Ser-28 and Pro-30 residues within a putative phospholipid bilayer binding site. Previously, we investigated the interaction of CTII with multilamellar liposomes of dipalmitoylphosphatidylglycerol by wide-line ^{31}P-NMR spectroscopy. To compare interactions of these proteins with phospholipids, we investigated the interaction of CTI with the multilamellar liposomes of dipalmitoylphosphatidylglycerol analogously. The effect of CTI on the chemical shielding anisotropy and deformation of the liposomes in the magnetic field was determined at different temperatures and lipid/protein ratios. It was found that both the proteins do not affect lipid organization in the gel state. In the liquid crystalline state of the bilayer they disturb lipid packing. To get insight into the interactions of the toxins with membranes, Monte Carlo simulations of CTI and CTII in the presence of the bilayer membrane were performed. It was found that both the toxins penetrate into the bilayer with the tips of all the three loops. However, the free-energy gain on membrane insertion of CTI is smaller (by $\approx$7 kcal/mol; 1 kcal $\equiv$ 4.184 kJ) when compared with CTII, because of the lower hydrophobicity of the membrane-binding site of CTI. These results clearly demonstrate that the P-type cytotoxins interact with membranes stronger than those of the S-type, although the mode of the membrane insertion is similar for both the types.

Key words: ^{31}P-NMR, membrane-binding mode, molecular hydrophobicity potential, Monte Carlo simulation, phospholipid, three-finger toxins.

INTRODUCTION

Cytotoxins (CTs) are small ($\sim$60 amino acids) proteins, which are abundant in the venom of the snakes of the Elapidae family. These basic proteins (approx. 9–12 lysine and arginine residues) possess haemolytic, cytotoxic activity and are capable of depolarizing membranes of myofibrils [1,2]. It has been suggested that such effects arise due to an ability of CTs to interact by a combination of electrostatic and hydrophobic forces with lipid and biological membranes [3]. In the experiments with model lipid membranes, it has been shown that CTs fuse phospholipid vesicles [4,5], induce phase separation in mixtures of anionic and zwitterionic phosphatidylcholines [6] and modify thermotropic characteristics of phospholipid membranes [7]. These studies have led to the division of the CTs into P- and S-type, which differ by the presence of either Pro-31(30) or Ser-29(28) residues respectively [8]. However, a gap still remains in understanding the relationship between their modes of interaction with membranes and biological activity.

To fill this gap, we studied binding modes of CTs and their effect on phospholipid bilayers. First, we studied in detail CTII from the venom of *Naja oxiana* (Central Asian cobra). Influence of CTII on thermotropic properties of anionic phospholipid membranes was determined earlier [7]. Later on, binding of CTII to phospholipid vesicles, its localization in detergent micelles [9] and bilayer membrane [10] were studied. Spatial structure of this toxin has been determined in aqueous solution [11] and in detergent micelles [9]. It has been shown that in the latter medium CTII conserves its three-finger scaffold. Loop II adopts an Ω-shape due to the presence of a tightly bound water molecule within its extremity. This loop combines the extremities of all the loops I–III into the hydrophobic stretch. It has been proposed that immersion of CTII in a DPPG (dipalmitoyl phosphatidylglycerol) bilayer is accomplished through the insertion of the above stretch into the interface region of the bilayer. This results in an increase in the membrane elastic modulus. Formation of an isotropic phase occurs when the lipid/protein ratio exceeds a threshold value [12].

To get further insight into the interaction of the three-finger toxins with phospholipid membranes, it is important to consider structurally related peptides, different from CTII by the charge and/or hydrophobicity. It is reasonable to consider CTI present in the same snake venom. On the basis of ^{1}H-NMR results, spatial structure of CTI was found to be nearly identical with that of CTII (M. A. Dubinnyi, Y. E. Pustovalova, P. V. Dubovskii, Yu. N. Utkin, A. G. Konshina, R. G. Efremov and A. S. Arseniev, unpublished work). Moreover, it has been shown recently [13] that both CTs conserve their secondary structure on interaction with negatively charged phospholipid membranes. Despite the structural similarity, these CTs are featured by different cytotoxicity and co-operativity of the interaction with human promyelocytic leukaemia cells HL60, murine monocytic cells WEHI-3 and human erythroleukaemic cells K562 [13].

The objective of the present work is to study the lipid–protein interactions for CTI with the experimental set-up used recently for CTII [12]. First, conditions at which this toxin is fully bound to MLV (multilamellar liposomes) of DPPG were found by ^{1}H-NMR spectroscopy. Then the response of MLV to the partitioning

Abbreviations used: *ASP*, atomic solvation parameter; CSA, chemical shift anisotropy; CT, cytotoxin; DPPG, dipalmitoyl phosphatidylglycerol; ISO, isotropic signal; L/P ratio, lipid-to-protein ratio; MC, Monte Carlo; MHP, molecular hydrophobicity potential; MLV, multilamellar liposomes.

[1] To whom correspondence should be addressed (email aars@nmr.ru).

The co-ordinates of CTI and CTII have been deposited with the Brookhaven Protein Data Bank under the accession numbers PDB 1RL5 and PDB 1CB9 respectively.

of the toxin was measured with ^{31}P-NMR spectroscopy: the CSA (chemical shift anisotropy) at the ^{31}P nucleus together with the deformation of the MLV in the magnetic field of the spectrometer. To understand possible differences in the lipid–protein interactions of the three-finger toxins at the molecular level, we investigated in detail their electrostatic and hydrophobic features. Also an ability of the toxins to insert into model membrane-mimic media was explored through MC (Monte Carlo) simulations. This was done using the hydrophobic slab model of the membrane developed earlier [14]. Previously, we have shown [15] that CTII is capable of inserting into the membrane through the hydrophobic tips of its three loops. In the present study, a similar approach was used for CTI. Moreover, the free-energy cost of the membrane insertion for both the toxins was estimated.

MATERIALS AND METHODS

Purification of the toxins

CTI was isolated and purified as described in [16]. It was additionally purified by the reversed-phase liquid chromatography using Vydac C_{18} column in the concentration gradient of acetonitrile in aqueous solution (from 15 to 45 % every 30 min) in the presence of 0.1 % of trifluoroacetic acid. According to the results of analytical reversed-phase HPLC, the content of the toxin in the purified preparations amounted to no less than 96 %.

Sample preparation

MLV of DPPG (Avanti Polar Lipids, Alabaster, AL, U.S.A.) were prepared by the addition to the lipid powder of the buffer: 0.2 M NaOAc (pH 5.5), 10 mM EDTA, 150 mM KCl in ^2H_2O (99.9 %; Izotop, St. Petersburg, Russia) with the required amount of the toxin (if necessary). NaOAc, EDTA and KCl were products of Reachim (Moscow, Russia). Water content in the samples for ^{31}P-NMR was kept at ^2H_2O/DPPG = 900:1 mol/mol (90–93 %, w/w). To homogenize the samples, thermocycling over the range 30–50 °C and mechanical agitation were used.

For ^{1}H-NMR experiments, 1 mg of CTI was dissolved in the 0.5 ml mixture of $^1H_2O/^2H_2O$ (470/30, v/v) containing 10 mM NaOAc (pH 5.5), 10 mM KCl and 1 mM EDTA. In the same buffer, MLV of DPPG were prepared (lipid concentration was 25 mM). The required L/P ratio (lipid-to-protein ratio) was attained after the addition of an aliquot of the lipid to the toxin solution followed by thorough stirring. In all NMR experiments, tubes (Norell, Landisville, NJ, U.S.A.) with outer diameter of 5 mm were used.

Acquisition of NMR spectra

NMR spectra were obtained on an 11.4 T Bruker DRX-500 spectrometer (Bruker, Karlsruhe, Germany) with ^{1}H- and ^{31}P-resonance frequencies at $\omega_0/2\pi = 500.13$ and 202.5 MHz respectively using a standard broadband 5 mm probe head. The magnetic field of the spectrometer was locked during acquisition through ^2H_2O contained in the samples. The temperature was controlled by the VT-system BVT 3000 to be within ± 0.1 °C. Chemical shifts were referenced to the external 85 % H_3PO_4 or internal $^1H^2HO$ signal in the ^{31}P- and ^{1}H-NMR spectra respectively. The WATERGATE scheme [17] was used for water signal suppression in the ^{1}H-NMR spectra. A spectral window of 7508 Hz/32 kB data points was used. The ^{31}P-NMR spectra were recorded with a spin echo sequence utilizing full phase cycling of both the transmitter and receiver [18]. A 90° pulse of 8 μs and an interpulse delay of 40 μs were used. The repetition time was 3–8 s, the longer time being used at higher temperatures. A total of 1000–3000 scans were accumulated for each spectrum of 60 606 Hz spectral width. During acquisition, broadband ^{31}P–^{1}H decoupling was applied. Spectral processing was performed with WINNMR software supplied by the spectrometer's manufacturer (Bruker). The free induction decays of 2 kB data points were zero-filled to 4 kB data points, multiplied by a Lorentzian (broadening factor of 50 Hz) and then Fourier-transformed.

Line-shape simulation

Theoretical ^{31}P-NMR spectra were calculated and fitted to the experimental spectra using the program Mathematica (version 4.0; Wolfram Research) as described before [12]. The adjustable parameters of the fitting were: components of the tensor of the CSA, integral intensity, the ratio of axes of ellipsoidal MLV, half-widths of Lorentzian or Gaussian line shapes and their proportion.

MC simulations in implicit membranes

MC simulations of the toxins in membrane-mimic environment were performed as follows. The co-ordinates for the starting structure of CTI and CTII were those obtained through NMR spectroscopy in aqueous solution (entry no. 1RL5 and 1CB9 respectively in the Brookhaven Protein Data Bank [19]). The membrane was represented with the model of a 'hydrophobic slab' [14]. Interactions of a protein with aqueous and membrane environment, as well as with membrane–water interface were described by an effective solvation potential based on *ASP*s (atomic solvation parameters) for gas–cyclohexane and gas–water transfer [20]. All-atom potential energy function for a protein was taken in the following form: $E_{\text{total}} = E_{\text{ECEPP/2}} + E_{\text{solv}}$. The term $E_{\text{ECEPP/2}}$ includes van der Waals, torsion, electrostatic, hydrogen and disulphide bonding contributions [21]. The solvation term (E_{solv}) was calculated according to the formula:

$$E_{solv} = \sum_{i=1}^{N} \Delta\sigma_i \; ASA_i$$

where ASA_i is the accessible surface area, $\Delta\sigma_i$ is the *ASP* of atom i and N is a number of protein atoms. Three independent MC simulations with different starting position of CTI relative to the membrane were performed.

In the beginning, the starting structures were placed in an aqueous phase arbitrarily. To change the orientation of the proteins with respect to the membrane during the simulation, fragments of 20 dummy residues were attached to their N-termini. Atoms of these residues had zero values of the force field parameters and, hence, did not contribute to the energy of the system. The first atom of the N-terminal dummy residue was always placed at the centre of the hydrophobic layer with the co-ordinate (0, 0, 0). All dihedral angles were sampled, except angles ω in 'real' residues. The choice of variable dihedral angles was made at random. Non-bond interactions were truncated with a spherical cut-off of 20 Å (1 Å = 0.1 nm). Electrostatic interactions were treated with distance-dependent dielectric permeability $\varepsilon = 4r$. At each MC step, the conformers were subjected to energy minimization, and then the selection was done according to the Metropolis criterion. To cross the energy barriers between local minima, the adaptive-temperature schedule method [22] was employed. The first 10^4 MC steps were performed with a set of NMR-derived distance constraints applied to the backbone atoms of residues involved in the secondary structure elements. Then, several consecutive MC runs (in total, approx. 2×10^4–2.5×10^4 MC steps) were performed without constraints. For each run, the initial conformation

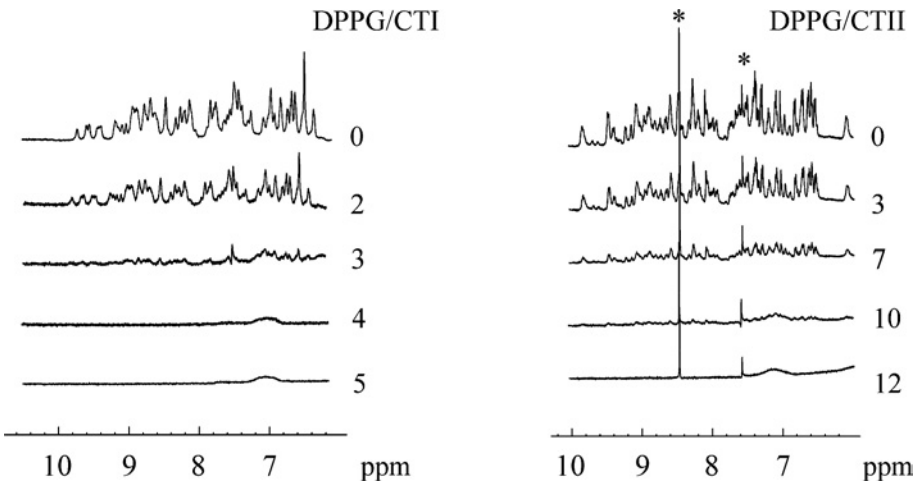

Figure 1 ^{1}H-NMR spectra of CTI (left) and CTII (right) in the presence of MLV of DPPG at 30 °C

The lipid/protein molar ratio is indicated next to the spectra. The impurity peaks are marked with the asterisks.

was the lowest-energy configuration found in the previous run. Other details of the implicit membrane model and MC computational methods were as described earlier [14,15,20].

To estimate the free-energy cost ($\Delta\Delta G$) of membrane insertion for CTI and CTII, the following computational method was developed. The starting structures for the toxins were the lowest-energy states found through MC search. Both of them represented membrane-bound states, where all three toxins' loops are immersed in the hydrophobic membrane layer [15]. Then a series of constant-temperature MC simulations for CTI and CTII was performed with gradual perturbation of the *ASP* describing solvation effects: from the original water–cyclohexane–water *ASP*s to water *ASP*s. In other words, the hydrophobic layer of the membrane was 'faded away' during the calculations. For each individual MC run, the system was equilibrated, and then the perturbations of *ASP*s for the accumulated ensemble of conformers were performed. Analysis of the averages obtained and subsequent integration along the path (membrane-to-water) permits estimation of the free-energy difference between the membrane-bound and water-solvated states [23]. Other details of the calculations will be published elsewhere.

Assessment of electrostatic and hydrophobic properties of toxins

For the resulting low-energy states of toxins, electrostatic potential energy (E_{el}) and MHPs (molecular hydrophobicity potentials) [24] on protein–solvent accessible surfaces were calculated. Spatial distribution of E_{el} was obtained from finite difference solutions to the Poisson–Boltzmann equation. The protein interior and surrounding solvent were assigned a dielectric constant of 2 and 80 respectively. The system was mapped on to a three-dimensional cubical grid, with spacing between grid points of 1 Å, and the Poisson–Boltzmann equation was numerically solved for the electrostatic potential. This was done using the DelPhi program [25]. MHP created by protein atoms on the solvent-accessible surface was calculated as described earlier [26]. The formalism of MHP utilizes a set of atomic physicochemical parameters evaluated from octanol–water partition coefficients of numerous chemical compounds [27]. The calculation and visualization of MHP was done using software written by the authors. Protein structures were drawn using the MOLMOL program [28].

RESULTS AND DISCUSSION

Binding of the toxins to membranes of DPPG: ^{1}H-NMR spectroscopy

To determine the range of L/P ratios at which CTI is completely bound to lipid, ^{1}H-NMR spectra of the toxin in aqueous solution were measured at temperatures 30–55 °C in the presence of the increasing amounts of MLV of DPPG (Figure 1). The increase in the lipid content of the samples resulted in the attenuation of the spectral lines until their complete disappearance due to an immobilization of the protein through binding to the lipid. As seen from Figure 1, the ^{1}H-NMR spectral lines of CTI vanish at L/P ratio of approx. 4:1. Therefore in further work, L/P ratios exceeding 5:1 were used to assure complete binding of CTI to DPPG.

It is necessary to indicate that the lowest L/P ratio at which the ^{1}H-NMR spectral lines of the toxins are substantially attenuated does not depend on temperature over the selected range of 30–55 °C. This was also observed for CTII [12] and might be due to a preponderance of electrostatic interactions in the binding of these toxins to the lipid. Indeed, hydrophobic interactions for CTII were found to be substantially dependent on the phase state of DPPG [12]. Moreover, under chosen ionic and hydration conditions, binding of CTI to zwitterionic dipalmitoylphosphatidylcholine was not observed (^{1}H-NMR spectra are not shown). The absence of the binding to dipalmitoylphosphatidylcholine was also observed for CTII [12]. It is interesting to note that the L/P ratio at which the full binding of CTI to negatively charged DPPG occurs is close to the formal charge of this toxin of +5 (at pH 5.5). This is also true for CTII (charge of +9).

^{31}P-NMR of MLV of DPPG in the presence of the toxins

Line shape of ^{31}P-NMR spectra of membranes is sensitive to anisotropic motions of phospholipid molecules falling on the timescale of approx. 10^{-2}–10^{-4} s [29]. Therefore it is sensitive to polymorphic transitions of phospholipids such as bilayer to hexagonal or isotropic phases [30–32]. Such transitions can be induced by CTI on interactions with MLV of DPPG (Figure 2). A typical 'bilayer-like' ^{31}P-NMR spectrum of MLV of pure DPPG at 50 °C (liquid crystalline state) (Figure 2a) is changed to the spectrum with a slightly reduced value of CSA and parameter *c*/*a* (deformation of liposomes; see details under the 'Influence of the toxins on the elastic properties of DPPG subsection') (Figure 2b). When the L/P

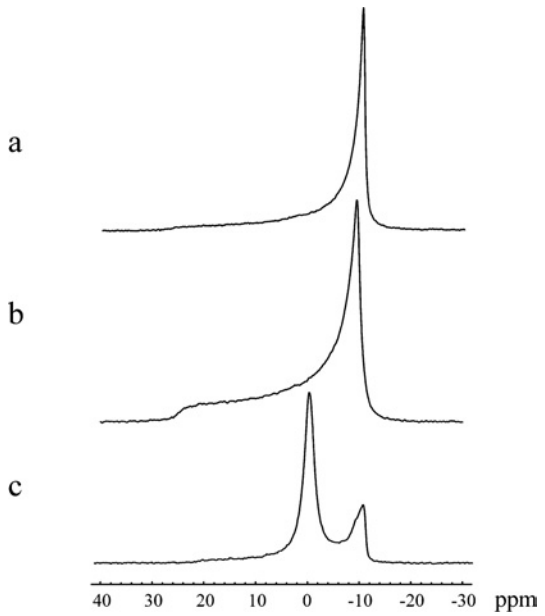

Figure 2 ^{31}P-NMR spectra of MLV DPPG at 50 °C in the absence of CTI (a) and in the presence of CTI at L/P ratios of 40:1 (b) and 10:1 (c)

The parameters of CSA ($\Delta\sigma$) at the ^{31}P nucleus of DPPG bilayer, the deformation (*c/a*) of the liposomes in the magnetic field and the content of isotropic signal estimated by computer simulation of the line shape were found to be respectively: (**a**) 38 ± 1 p.p.m., 1.90 ± 0.05, 0 %; (**b**) 35 ± 1 p.p.m., 1.49 ± 0.05, 0 % and (**c**) 30 ± 1 p.p.m., 1.15 ± 0.05, 78 ± 1 %.

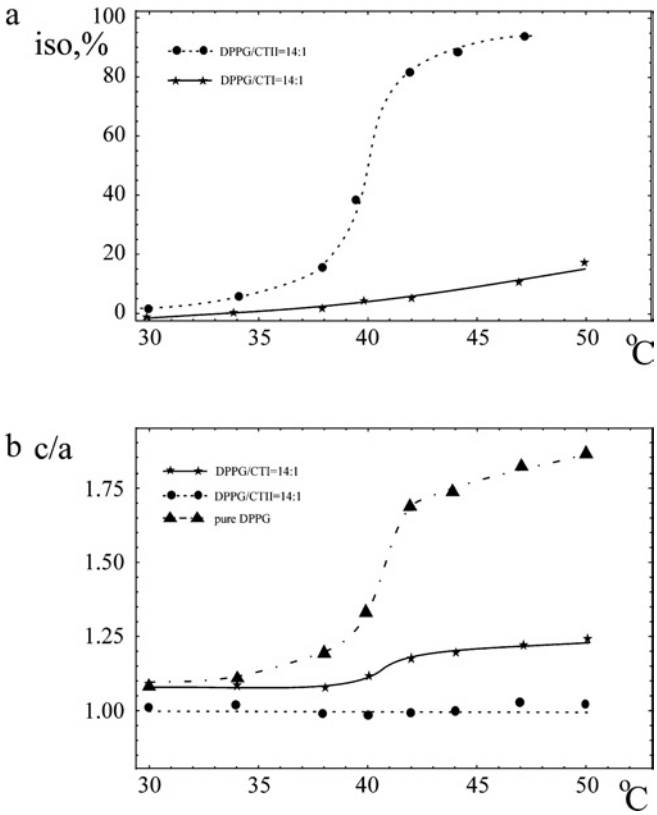

Figure 3 Temperature dependence of (a) the content of ISO (%) in the ^{31}P-NMR spectra of MLV DPPG in the presence of CTI (continuous line) or CTII (broken line) and (b) the deformation of the liposomes in the presence or absence of these toxins

ratio is decreased below 15:1, the isotropic signal is present in the ^{31}P-NMR spectra (Figure 2c). The corresponding isotropic phase was attributed to the electrically neutral lipid−toxin complexes [33]. They are featured by the specific stoichiometry, i.e. L/P ratio at which the total charge of the toxin molecule is neutralized with a certain number of lipid molecules.

In Figure 3(a), temperature dependence of the content of the ISO (isotropic signal) in the ^{31}P-NMR spectra of DPPG/CTI (14:1) mixture is shown. For comparison, the corresponding dependence for CTII [12] is also shown. As seen from Figure 3, at the L/P ratio of 14:1 for CTI, ISO is practically not observed at $T < T_p$ (where $T_p \sim 41$ °C, the temperature of the gel-to-liquid crystalline transition of DPPG). At $T > T_p$, the ISO value for CTI is approx. 10 times lower than that observed for CTII. For CTII, as opposed to CTI, a sigma-shaped dependence of ISO is observed. The ISO value is increased by 70 % in the narrow temperature interval of 38–42 °C encompassing T_p. It is clearly evident that partitioning of CTII is critically dependent on the phase state of the bilayer and thus on the 'free space' between phospholipid head groups.

The dependence of the ISO value on the L/P ratio is shown in Figure 4(a). It increases almost linearly with decrease in L/P ratio for CTII below 20:1. The same trend was observed for CTI (Figure 4a). However, a threshold L/P ratio at which the growth of the isotropic signal begins is shifted towards lower values (∼15:1). At 50 °C, the pure isotropic phase is formed at an L/P ratio of approx. 10:1 for CTII and approx. 6:1 for CTI (Figure 4a). Such a difference may be attributed to a difference in the net electrical charge of these toxins (+9 and +5 at pH 5.5 respectively) and thus on the stoichiometry of lipid–toxin complexes.

Anisotropy of the chemical shift

No influence on CSA was observed in the gel state of DPPG (below ∼41 °C) in the presence of CTI. Previously, this was also observed for CTII [12]. In the liquid crystalline state, such an influence was observed for CTI as opposed to CTII. To illustrate this, the dependence of CSA values on the L/P ratio for CTI/DPPG mixtures at 50 °C is presented in Figure 4(b). It is seen that the decrease in L/P ratio from 100:1 to 10:1 diminishes the absolute value of CSA by approx. 7 p.p.m. In contrast, the corresponding values for CTII/DPPG in the gel (30 °C) and liquid crystalline (50 °C) states (Figure 4b) (59 ± 2 and 37 ± 1 p.p.m. respectively) were found to coincide with the respective values for the pure DPPG dispersions. The ability of the three-finger toxins to induce a comparable decrease in CSA values at the ^{31}P-nucleus of zwitterionic [34] and anionic [33] phospholipid membranes in the liquid crystalline state was previously described. The observation of such an effect for CTI and its absence for CTII might indicate that only CTI but not CTII is capable of inducing changes in the motional freedom of the headgroup of the phospholipid [35]. The molecular basis of these differences is assessed in the following sections.

Influence of the toxins on the elastic properties of DPPG

Molecules of phospholipids are featured by the diamagnetic anisotropy and their assemblies are able to reorient themselves in the magnetic field [36–38]. As a result, MLV are stretched along the direction of the applied magnetic field and adopt an ellipsoidal shape [39]. On binding to the surface of MLV, proteins may influence bending elastic modulus of the lipid membrane and hence the extent of the deformation of the liposomes in the magnetic field [40]. This is manifested as a redistribution of the intensities between up-field peak and low-field shoulder in the bilayer-type ^{31}P-NMR spectra of the membranes [39]. Computer

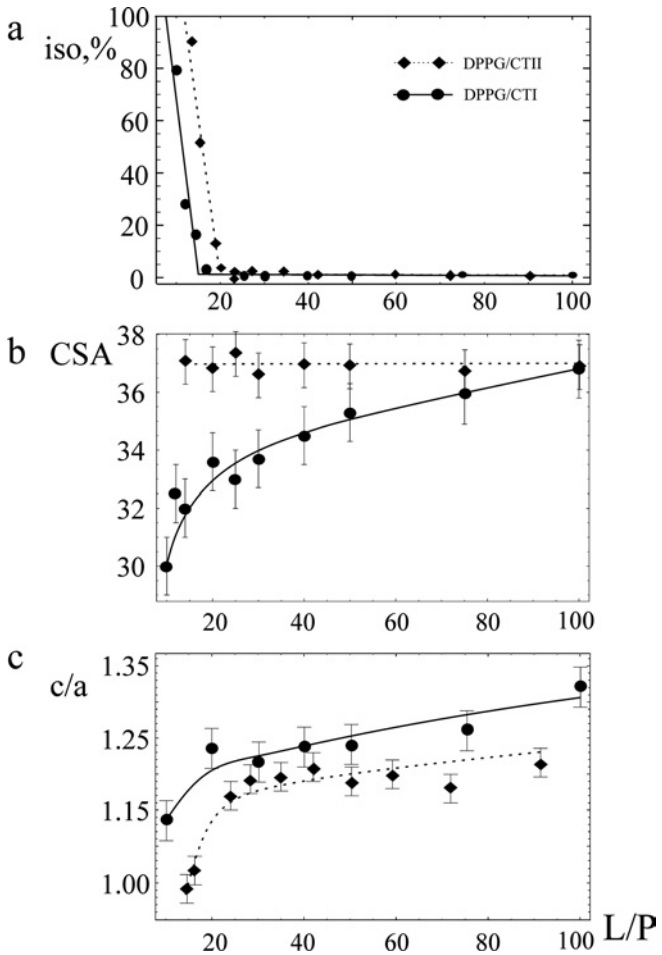

Figure 4 Dependence of the response of MLV of DPPG to CTI (continuous line) and CTII (broken line) on L/P ratio evaluated by computer decomposition of the line shape of the ^{31}P-NMR spectra at 50 °C: (a) content of isotropic phase, (b) CSA value and (c) *c*/*a* of MLV

simulations of the ^{31}P-NMR spectra (see the Materials and methods section) allow extraction of the ratio of the axes of the ellipsoid (*c*/*a*).

As shown previously, CTII influences the deformation of MLV of DPPG in the magnetic field of the spectrometer [12]. When the amount of CTII bound to DPPG increased, the deformation of MLV decreases. It seems that this is due to the increase in the bending elastic modulus of DPPG bilayer on incorporating CTII. The dependence of deformation of DPPG liposomes by CTI or CTII on the L/P ratio is shown in Figure 4(c). When the ratio DPPG/CTII reached approx. 14:1, the deformation of MLV at $T > T_p$ is not observed, i.e. liposomes became spherical ($c/a \sim 1$) (Figure 4c). The values of deformation (*c*/*a*) of liposomes with CTI binding exhibit higher values in the whole range of L/P ratios (at 50 °C) (Figure 4c).

Temperature dependence of *c*/*a* values of DPPG liposomes in the presence of CTI and CTII at the selected L/P ratio of 14:1 is shown in Figure 3(b). Over the temperature range studied (30–50 °C), CTII prevents deformation of MLV of DPPG to a greater extent when compared with CTI. A decrease in DPPG/CTI ratio resulted in decrease in *c*/*a* values for the whole temperature range. However, even at an L/P ratio above 100:1, the curve does not coincide with that for pure DPPG (results not shown). Thus the effect of CTI on *c*/*a* value of MLV of DPPG is detectable even at high dilution of the toxin with lipid as was observed for CTII [12]. For the latter toxin, it was suggested that the gel-to-liquid crystalline transition of DPPG promotes penetration of the toxin into the hydrophobic region of the bilayer [12]. The following sections disclose a possible molecular basis for the above experimental results.

Electrostatic properties of the toxin molecules

The calculated distributions of electrostatic potential (E_{el}) on the toxins' surfaces are shown in Figure 5. Comparative analysis of E_{el} for both CTs indicates a high degree of their similarity, although several important differences are to be noticed. Surfaces of both the toxins reveal an extensive region located above the hydrophobic tips of the loops, which is characterized by high positive values of E_{el}. In other words, the conservative positively charged lysine and arginine residues (Lys-5, 12, 23, 35, 44, 50 and Arg-36) form a polar 'belt' on the surface of CTs (Figure 5). The surface regions near the tips of the three loops of CTs display low positive (close to zero) values of E_{el}. On the other hand, in the vicinity of the loop II of CTI there is a negatively charged zone created by Ser-28 and Asp-29. This is not the case for CTII. In its sequence, these positions are occupied by alanine residues (Figure 5). Moreover, the surface of CTII near the tip of loop I is characterized by a uniform distribution of low positive values of E_{el}, whereas in CTI this region is negatively charged.

To summarize, the analysis of electrostatic properties of the surface of CTs leads to the following conclusions: (i) the presence of the extensive region with high positive values of E_{el} seems to be favourable for 'sealing' of the toxins on the negatively charged bilayer surface; (ii) it is quite probable that the membrane-binding motif is formed by the hydrophobic residues from the tips of the loops I–III, because the corresponding protein surface is almost electrically neutral; and (iii) as distinct from CTII, the negatively charged zone on the surface of the loop II impedes the interaction of CTI with the anionic bilayer; this observation is consistent with the experimental results described above.

MC simulations of toxins in the implicit model membrane

Previously, we have developed an implicit hydrophobic slab model, which mimics the effects of membrane in MC simulations of peptides and proteins [14]. The method has been successfully applied to a number of polypeptides with different folds [14,15]. To assess the spatial structure and to compare parameters of membrane binding for both CTs in this study, we employed the aforementioned approach to CTI. Similar to CTII, CTI protrudes into the membrane through the hydrophobic tips of the three loops: residues 5–10 (loop I), 24–36 (loop II) and 46–50 (loop III). Also, both the proteins are found to retain their overall three-dimensional structures after binding to the membrane. The results of the simulation are in good agreement with the spectroscopic results on CTII and CTI in model membranes [13]. On the other hand, a similar mode of membrane binding obtained for CTI and CTII in a hydrophobic slab does not permit delineation of subtle differences in behaviour of these toxins at the water–bilayer interface. To solve the problem, it was proposed to estimate the difference in 'free-energy' ($\Delta\Delta G$) between the membrane-bound and water-solvated states of CTI and CTII (see the Materials and methods section). In the present study, the term 'energy' is referred to as the sum of the internal energy of the protein and the energy arising from the interaction of protein with heterogeneous membrane-mimic media (E_{solv}), whereas the energy of the membrane itself is considered to be constant.

Analysis of the low-energy states found by MC conformational search revealed that $\Delta\Delta G$ values are -6.8 and -14.1 kcal/mol

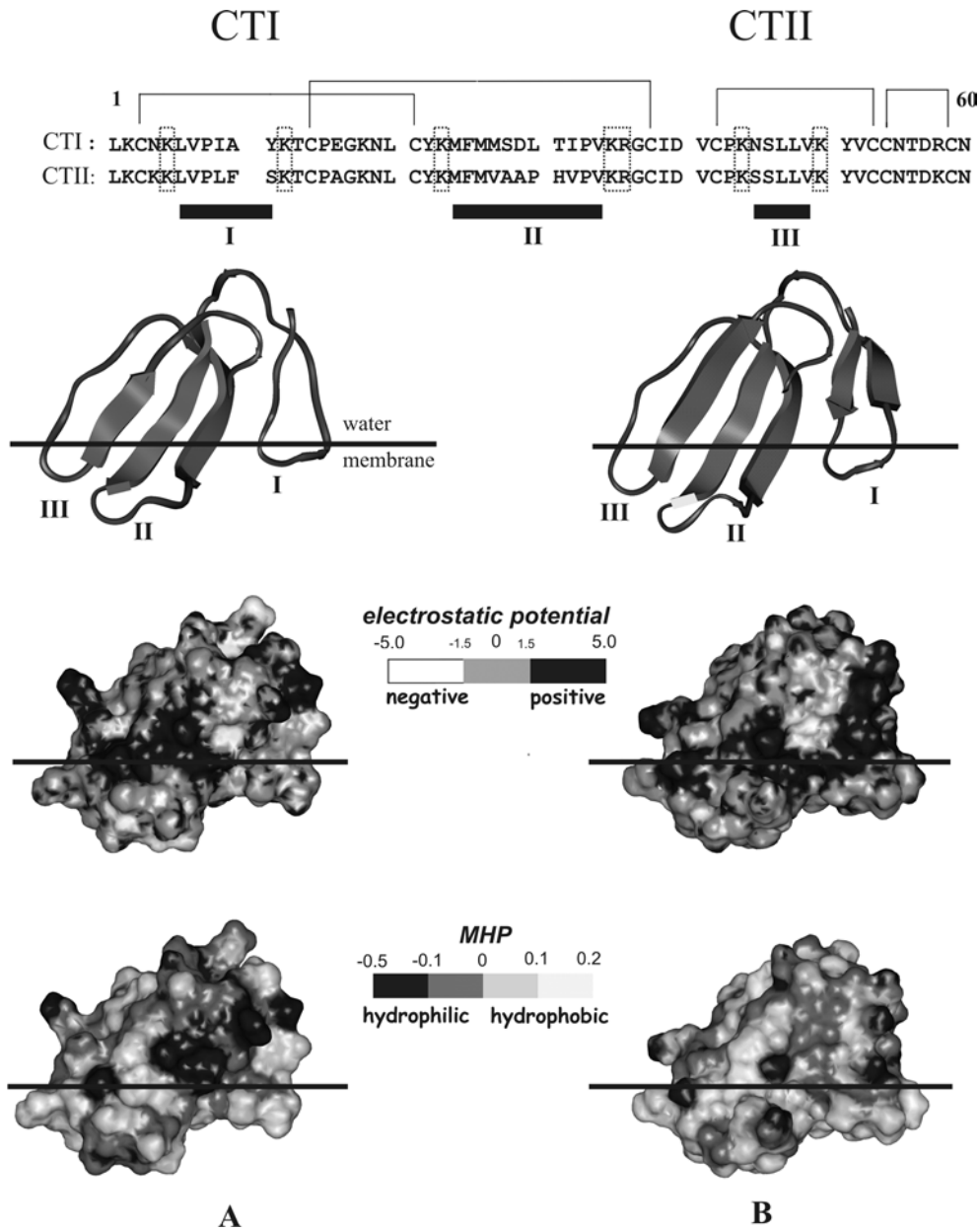

Figure 5 Amino acid sequences and spatial structures of CTI (left) and CTII (right) (the co-ordinates of CTI and CTII deposited to the Protein Data Bank are 1RL5 and 1CB9 respectively) with distribution of electrostatic (E_{el}) potential and MHP

The disulphide bridges and numbering of residues are indicated above the sequences. The loops are designated with roman numbers below the sequences and in the structures. The charged residues encircling the loops are enclosed in boxes. Protein structures are given in a ribbon presentation and correspond to the lowest-energy states found by MC simulations of CTs in the membrane. The hydrophobic–hydrophilic interface of the membrane is indicated by a horizontal line. All the views are given for the same orientation of the toxin molecules. The solvent-accessible surfaces are shaded according to the E_{el} and MHP values. The E_{el} and MHP scales are given by the corresponding bars. The E_{el} values are given in units of $\boldsymbol{k}T/e$ (where $\boldsymbol{k}$ is the Boltzmann constant, T the temperature and e the electron charge). The MHP values are given in conventional units.

(1 cal = 4.184 J) for CTI and CTII respectively. Therefore CTII binds to the membrane more strongly than CTI, although their modes of insertion are very similar. This demonstrates high efficiency of the new computational approach to 'fish out' differences in membrane-binding capacity for conformationally rigid proteins. This last enquiry is important because, in the calculations of $\Delta\Delta G$, thermodynamic aspects of molecular lability are not considered. Considering that the spatial structures of CTs do not change significantly on the membrane insertion, it is reasonable to suggest that the binding capacity of the toxins is governed by polarity properties of their solvent-exposed surfaces. That is why in the next section we present comparative analysis of the hydrophobic properties of the molecules of CTI and CTII.

Distribution of polarity and hydrophobicity properties on the accessible surface of toxins

The MHP created by protein atoms on the solvent-accessible surface was used as a measure of the toxins' polarity. Figure 5 shows three-dimensional surfaces of the toxins mapped according

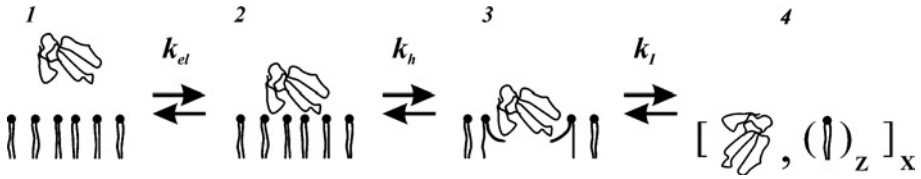

Figure 6 Schematic representations of the modes of binding of the three-finger toxins to lipid membranes

Only the upper leaflet of the bilayer is shown. The number of lipid molecules in the figure does not decrypt stoichiometry of the toxin–lipid interaction. See the text for details.

to MHP values. The surface regions with negative and positive values of MHP correspond to hydrophilic and hydrophobic areas respectively. As seen in Figure 5, in both CTs the regions of the surface near the tips of the loops I–III form an extended hydrophobic 'bottom', by which the toxins are docked on the membrane–water interface. Previously, we have shown that in the case of CTII, significant decrease in E_{solv} occurs when the toxin inserts into the non-polar layer of the model membrane [15]. This means that to reach the most energetically favourable state, CTII interacts with the membrane instead of staying in aqueous solution. The same is also true for CTI.

At the same time, in spite of the overall similarity in hydrophobicity of CTs' surfaces, there are some important differences in the details of MHP distribution. In comparison with CTII (which belongs to the P-type CTs), the tips of the loops I and II in CTI (the S-type CT) are less hydrophobic due to the replacements $Phe^{10} \rightarrow Ala$, $Ala^{28} \rightarrow Ser$ and $Ala^{29} \rightarrow Asp$ (Figure 5). The residues Ser-28 and Asp-29 of CTI form a polar region with low MHP values between the loops I and III (Figure 5). So, the putative membrane-binding site ('hydrophobic bottom') is more polar in CTI. We should note that the surface of CTII also contains a polar region near the tip of loop II (formed by His-31). However, it is located above the main pattern of hydrophobicity; in the membrane-bound conformations found by MC simulations, this site occupies an interfacial position and interacts with a relatively polar environment.

Interaction of three-finger toxins with lipid membranes: combined view

Taking into account the experimental results on the interaction of the three-finger toxins with lipid membranes and considering their molecular properties studied with molecular modelling techniques, the following picture emerges (Figure 6).

The binding of the peptides to negatively charged membranes requires involvement of electrostatic forces that bring about the sorption of the peptides to the membrane surface (Figure 6, the transition from $1 \rightarrow 2$). Although, in the scheme, the liquid crystalline state of the membrane is implied, the $1 \rightarrow 2$ transition (Figure 6) is realized for the membrane in the gel state as well. It is probable that the equilibrium constant of this process (k_{el}) is poorly dependent on the phase state of the membrane but is governed mainly by the electrical charges of the peptide and membrane. For electrically neutral membranes, the sorption of the peptides was not observed.

A peptide that is attracted to the lipid–water interface due to electrostatic interaction then partitions into the membrane hydrophobically [41]. This notion is true for both the toxins and DPPG membrane in the liquid crystalline state. This is mainly due to the fact that CTs possess the hydrophobic patch within the extremities of the three fingers. The depth of their hydrophobic penetration into the membrane–water interface is limited by the polar belt formed by homologous positively charged lysine and arginine residues (Figure 5). The insertion process is described by the constant of hydrophobic binding k_h. This constant depends on the hydrophobic surface of molecules embedded into the hydrophobic portion of the membranes [41]. Therefore the equilibrium is more noticeably shifted towards state 3 for CTII when compared with CTI. As a result, the influence of CTI on the deformation of the liposomes of DPPG in the magnetic field is less prominent when compared with that for CTII.

The accumulation of the penetrated states of the toxins within a membrane results in the attainment of the critical concentration of the peptide above which the bilayer structure of the membrane is deteriorated. The isotropic phase (state 4) is formed and its formation is described by the equilibrium constant k_l. Among the factors that influence k_l, we may indicate the ability of the peptides to modulate the curvature of the lipid surface [42]. This property is dependent on the position of the peptide molecule with respect to the lipids and on the organization of different membrane phospholipids such as their 'molecular shape' [31]. It is probable that such an ability depends on a combination of electrostatic and hydrophobic properties of CTs leading to the formation of electrically neutral stoichiometrical complexes of the toxin molecules with phospholipids [33].

The transitions between the states represented in Figure 6 is reflected in the following changes of the ^{31}P-NMR spectra. If state 1 corresponds to the ^{31}P-NMR spectrum of MLV in the absence of toxins, then state 2 is solely characterized by the changes in CSA value. This state was not observed in the pure form of either CTI or CTII. However, it is practically absent for CTII bound to liquid crystalline DPPG. State 3 is featured by the undistorted CSA value. However, the parameter c/a of the deformation of the liposomes is changed. It was observed previously for CTII. State 4 is represented with the ^{31}P-NMR spectrum containing only isotropic signals. This state was observed for both the toxins.

Thus, in the present study, we juxtaposed the experimental results on the interaction of the three-fingered toxins isolated from *N. oxiana* snake venom and their molecular properties evaluated by computer modelling techniques. The ^{31}P-NMR spectra of DPPG membranes in the presence of either CTI or CTII suggest that the membranes sense the binding of the toxins differently. The modes of binding of toxins to lipid membranes were proposed, although a number of experimental facts received no theoretical explanation. In particular, the theoretical model deals with neither the phase state of the lipid bilayer (gel or liquid crystalline) nor the formation of new lipid states (i.e. isotropic phase) or possible toxin–toxin interactions. Nevertheless, considering the properties of the toxin molecules only, it was concluded that the specific distribution of hydrophobic and hydrophilic residues over the surface of toxin molecules induces considerable changes in their ability for this insertion into the lipid bilayer. We should emphasize that the distribution of non-polar residues, which are favourable for embedding into the membrane, depends not only on the

amino acid composition, but is also sensitive to spatial configuration and arrangement of the loops (especially loops I and II) within CTs [43]. Thus, both CTs have a typical Ω-like shape of loop II, which is present in all the experimentally derived three-dimensional structures of CTs that are reported to interact with membranes [44]. Such a shape allows for the hydrophobic tips of the loops I and II to be placed at about the same distance from the membrane plane, and increases their area of contact with the membrane. This results in the formation of an extended and continuous domain with a high hydrophobicity potential on the protein surface ('hydrophobic bottom').

The proposed computational approach allows a detailed characterization of the electrostatic and hydrophobic features of accessible surfaces of proteins. Along with the results obtained by MC simulations in implicit membranes, the experimental results imply that the P-type CTs interact with membranes more strongly than those of the S-type although the mode of the membrane insertion is similar for both the types.

This work was supported partially by the Ministry of Education and Science of Russian Federation (the State contract 43.073.1.1.1508/31.01.2002, grant SS-1522.2003.4), by the Programme RAS MCB and by the Russian Foundation for Basic Research (RFBR), grant 02-04-48882-a and 04-04-48875-a. R. G. E. is grateful to the Science Support Foundation (Russia) for the grant awarded. Dr D. E. Nolde is acknowledged for help with $\Delta\Delta G$ calculations. Professor V. V. Chupin is thanked for valuable comments on the manuscript.

REFERENCES

1 Dufton, M. J. and Hider, R. C. (1988) Structure and pharmacology of elapid cytotoxins. Pharmacol. Ther. **36**, 1–40
2 Fletcher, J. E., Hubert, M., Wieland, S. J., Gong, Q.-H. and Jiang, M.-S. (1996) Similarities and differences in mechanisms of cardiotoxins, melittin and other myotoxins. Toxicon **34**, 1301–1311
3 Vincent, J. P., Balerna, M. and Lazdunski, M. (1978) Properties of association of cardiotoxin with lipid vesicles and natural membranes. A fluorescence study. FEBS Lett. **85**, 103–108
4 Aripov, T. F., Gasanov, S. E., Salakhutdinov, B. A., Rozenstein, I. A. and Kamaev, F. G. (1989) Central Asian cobra venom cytotoxins-induced aggregation, permeability and fusion of liposomes. Gen. Physiol. Biophys. **8**, 459–474
5 Chien, K. Y., Huang, W. N., Jean, J. H. and Wu, W. G. (1991) Fusion of sphingomyelin vesicles induced by proteins from Taiwan cobra (Naja naja atra) venom. Interactions of zwitterionic phospholipids with cardiotoxin analogues. J. Biol. Chem. **266**, 3252–3259
6 Carbone, M. A. and Macdonald, P. M. (1996) Cardiotoxin II segregates phosphatidylglycerol from mixtures with phosphatidylcholine: ^{31}P and ^{2}H NMR spectroscopic evidence. Biochemistry **35**, 3368–3378
7 Aripov, T. F., Rozenstein, I. A., Salakutdinov, B. A., Lev, A. A. and Gotlib, V. A. (1987) The influence of cytotoxins from central Asian cobra venom and melittin from bee venom on the thermodynamic properties of phospholipid bilayer. Gen. Physiol. Biophys. **6**, 343–357
8 Chien, K.-Y., Chiang, C.-M., Hseu, Y.-C., Vyas, A. A., Rule, G. S. and Wu, W. (1994) Two distinct types of cardiotoxin as revealed by the structure and activity relationship of their interaction with zwitterionic phosholipid dispersions. J. Biol. Chem. **269**, 14473–14483
9 Dubovskii, P. V., Dementieva, D. V., Bocharov, E. V., Utkin, Y. N. and Arseniev, A. S. (2001) Membrane binding motif of the P-type cardiotoxin. J. Mol. Biol. **305**, 137–149
10 Dubinnyi, M. A., Dubovskii, P. V., Utkin, Y. N., Simonova, T. N., Barsukov, L. I. and Arseniev, A. S. (2001) ESR study of the interaction of cytotoxin II with model membranes. Russian J. Bioorg. Chem. **27**, 102–113
11 Dementieva, D. V., Bocharov, E. V. and Arseniev, A. S. (1999) Two forms of cytotoxin II (cardiotoxin) from Naja naja oxiana in aqueous solution. Spatial structures with tightly bound water molecules. Eur. J. Biochem. **263**, 152–162
12 Dubovskii, P. V., Lesovoy, D. M., Dubinnyi, M. A., Utkin, Y. N. and Arseniev, A. S. (2003) Interaction of the P-type cardiotoxin with phospholipid membranes. Eur. J. Biochem. **270**, 2038–2046
13 Feofanov, A. V., Sharonov, G. V., Dubinnyi, M. A., Astapova, M. V., Kudelina, I. A., Dubovskii, P. V., Rodionov, D. I., Utkin, Y. N. and Arseniev, A. S. (2004) Comparative study of structure and activity of cytotoxins from Naja oxiana, Naja kaouthia and Naja haje cobra venom. Biochemistry (Moscow) **69**, 1148–1157
14 Efremov, R. G., Volynsky, P. E., Nolde, D. E. and Arseniev, A. S. (2001) Implicit two-phase solvation model as a tool to assess conformation and energetics of proteins in membrane-mimic media. Theor. Chem. Acc. **106**, 48–54
15 Efremov, R. G., Volynsky, P. E., Nolde, D. E., Dubovskii, P. V. and Arseniev, A. S. (2002) Interaction of cardiotoxins with membranes: a molecular modeling study. Biophys. J. **83**, 144–153
16 Grishin, E. V., Sukhikh, A. P., Adamovich, T. B. and Ovchinnikov, Yu A. (1976) Isolation, properties and sequence determination of the two cytotoxins from the venom of the Middle-Asian cobra Naja Naja oxiana. Bioorg. Khim. **2**, 1018–1034
17 Piotto, M., Saudek, V. and Sklenář, V. (1992) Gradient tailored excitation for single-quantum NMR spectroscopy of aqueous solutions. J. Biomol. NMR **2**, 661–665
18 Rance, M. and Byrd, R. A. (1983) Obtaining high-fidelity spin $^1/_2$-powder spectra in anisotropic media: phase cycled Hahn echo spectroscopy. J. Magn. Reson. **52**, 221–240
19 Berman, H. M., Westbrook, J., Feng, Z., Gilliland, G., Bhat, T. N., Weissig, H., Shindyalov, I. N. and Bourne, P. E. (2000) The Protein data bank. Nucleic Acids Res. **28**, 235–242
20 Efremov, R. G., Nolde, D. E., Vergoten, G. and Arseniev, A. S. (1999) A solvent model for simulations of peptides in bilayers. I. Membrane-promoting α-helix formation. Biophys. J. **76**, 2448–2459
21 Némethy, G., Pottle, M. S. and Scheraga, H. A. (1983) Energy parameters in polypeptides. 9. Updating of geometrical parameters, nonbonded interactions, and hydrogen bond interactions for the naturally occurring amino acids. J. Phys. Chem. **87**, 1883–1887
22 Von Freyberg, B. and Braun, W. (1991) Efficient search for all low energy conformations of polypeptides by Monte Carlo methods. J. Comp. Chem. **12**, 1065–1076
23 Mezei, M. and Beveridge, D. L. (1986) Free energy simulations. Ann. N.Y. Acad. Sci. **482**, 1–23
24 Furet, P., Sele, A. and Cohen, N. C. (1988) 3D molecular lipophilicity potential profiles: a new tool in molecular modeling. J. Mol. Graphics **6**, 182–200
25 Honig, B., Sharp, K. A. and Yang, A.-S. (1993) Macroscopic models of aqueous solutions: biological and chemical applications. J. Phys. Chem. **97**, 1101–1109
26 Efremov, R. G. and Vergoten, G. (1995) Hydrophobic nature of membrane-spanning α-helical peptides as revealed by Monte Carlo simulations and molecular hydrophobicity potential analysis. J. Phys. Chem. **99**, 10658–10666
27 Viswanadhan, V. N., Ghose, A. K., Revankar, G. R. and Robins, R. K. (1989) Atomic physicochemical parameters for three-dimensional structure directed quantitative structure-activity relationships. 4. Additional parameters for hydrophobic and dispersive interactions and their application for an automated superposition of certain naturally occurring nucleoside antibiotics. J. Chem. Inf. Comput. Sci. **29**, 163–172
28 Koradi, R., Billiter, M. and Wütrich, K. (1996) MOLMOL: a program for display and analysis of macromolecular structures. J. Mol. Graphics **14**, 51–55
29 Watts, A. (1998) Solid-state NMR approaches for studying the interaction of peptides and proteins with membranes. Biochim. Biophys. Acta **1376**, 297–318
30 Seelig, J. (1978) ^{31}P Nuclear magnetic resonance and the head group structure of phospholipids in membranes. Biochim. Biophys. Acta **515**, 105–140
31 De Kruijff, B., Cullis, P. R., Verkleij, A. J., Hope, M. J., van Echteld, C. J. A., Taraschi, T. F., van Hoogeveste, P., Killian, J. A., Rietveld, A. and van der Steen, A. T. M. (1985) Modulation of lipid polymorphism by lipid-protein interactions. In Progress in Protein-Lipid Interactions, vol. 1 (Watts, A. and De Pont, J. J. H. H. M., eds.), pp. 89–142, Elsevier, Amsterdam
32 Batenburg, A. M., Bougis, P. E., Rochat, H., Verkleij, A. J. and de Kruijff, B. (1985) Penetration of a cardiotoxin into cardiolipin model membranes and its implications on lipid organization. Biochemistry **24**, 7101–7110
33 Picard, F., Pezolet, M., Bougis, P. E. and Auger, M. (1996) Model of interaction between a cardiotoxin and dimyristoylphosphatidic acid bilayers determined by solid-state ^{31}P NMR spectroscopy. Biophys. J. **70**, 1737–1744
34 Sue, S.-C., Rajan, P. K., Chen, T.-S., Hsieh, C.-H. and Wu, W. (1997) Action of Taiwan cobra cardiotoxin on membranes: binding modes of a β-sheet polypeptide with phosphatidylcholine bilayers. Biochemistry **36**, 9826–9836
35 Pott, T., Mailett, J.-C. and Dufourc, E. J. (1995) Effects of pH and cholesterol on DMPA membranes: a solid state ^{2}H- and ^{31}P-NMR study. Biophys. J. **69**, 1897–1908
36 Qiu, X., Mirau, P. A. and Pidgeon, C. (1993) Magnetically induced orientation of phosphatidylcholine membranes. Biochim. Biophys. Acta **1147**, 59–72
37 Seelig, J., Borle, F. and Cross, T. A. (1985) Magnetic ordering of phospholipid membranes. Biochim. Biophys. Acta **814**, 195–198
38 Speyer, J. B., Sripada, P. K., Das Gupta, S. K., Shipley, G. and Griffin, R. G. (1987) Magnetic orientation of sphingomyelin-lecithin bilayers. Biophys. J. **51**, 687–691
39 Brumm, T., Möps, A., Dolainsky, C. and Bayerl, T. M. (1992) Macroscopic orientation effects in broadline NMR-spectra of model membranes at high magnetic field strength. A method preventing such effects. Biophys. J. **61**, 1018–1024

40 Picard, F., Paquet, M. J., Levesque, J., Belanger, A. and Auger, M. (1999) ^{31}P NMR first spectral moment study of the partial magnetic orientation of phospholipid membranes. Biophys. J. **77**, 888–902
41 Beschiaschvili, G. and Seelig, J. (1990) Melittin binding to mixed phosphatidylglycerol/phosphatidylcholine membranes. Biochemistry **29**, 52–58
42 Batenburg, A. M. and de Kruijff, B. (1988) Modulation of membrane surface curvature by peptide-lipid interactions. Biosci. Rep. **8**, 299–307
43 Konshina, A. G., Volynsky, P. E., Arseniev, A. S. and Efremov, R. G. (2003) Interaction of cardiotoxin A5 with membrane: role of conformational heterogeneity and hydrophobic properties. Russian J. Bioorg. Chem. **29**, 523–533
44 Sun, Y.-J., Wu, W., Chiang, C.-M., Hsin, Y.-A. and Hsiao, C.-D. (1997) Crystal structure of cardiotoxin V from Taiwan cobra venom: pH-dependent conformational change and a novel membrane-binding motif identified in the three-finger loops of P-type cardiotoxin. Biochemistry **36**, 2403–2413

Received 29 October 2004/6 December 2004; accepted 7 December 2004
Published as BJ Immediate Publication 7 December 2004, DOI 10.1042/BJ20041814